THE JOURNAL OF PHYSICAL CHEMISTRY B

Article

pubs.acs.org/JPCB

Functional Compartmental Modeling of the Photosystems in the Thylakoid Membrane at 77 K

Joris J. Snellenburg, Jan P. Dekker, Rienk van Grondelle, and Ivo H. M. van Stokkum*

Institute for Lasers, Life and Biophotonics, Faculty of Sciences, VU University Amsterdam, De Boelelaan 1081, 1081 HV, Amsterdam, The Netherlands

Supporting Information

ABSTRACT: Time-resolved fluorescence spectroscopy measurements at 77 K on thylakoid membrane preparations and isolated photosynthetic complexes thereof were investigated using target analysis with the aim of building functional compartmental models for the photosystems in the thylakoid membrane. Combining kinetic schemes with different spectral constraints enabled us to resolve the energy transfer pathways and decay characteristics of the different emissive species. We determined the spectral and energetic properties of the red Chl pools in both photosystems and quantified the formation of LHCII-LHCI-PSI supercomplexes in the transition from native to unstacked thylakoid membranes.

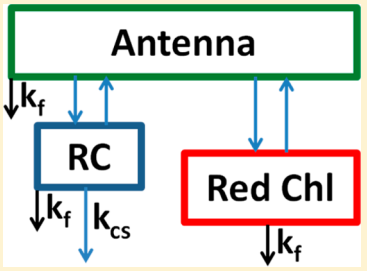

INTRODUCTION

In oxygenic photosynthesis, photosystem I (PSI) and photosystem II (PSII) bound to the thylakoid membrane convert light into chemically stored energy. Functional studies of the isolated photosynthetic complexes and the thylakoid membrane using time-resolved fluorescence spectroscopy[1] have provided us with a wealth of information on the elementary chemical and physical processes constituting the light reactions.[2,3] In isolated PSI cores equilibration between bulk Chl a and red Chl a, species with red-shifted emission relative to that of the reaction center (RC), precedes trapping in the RC, for example, as in refs 4−10. Larger complexes of PSI cores with LHCI antennae show even more complex dynamics, since the antennae also contain red Chl a species.[11−17] The core of PSII also contains species with red-shifted emission relative to that of the RC. In PSII the red Chl are less red-shifted (up to 696 nm) than in PSI (up to 740 nm). Depending upon the size of the PSII particle, different trapping time scales are found, in addition to spectral evolution related to the red Chl, for example, as in refs 18−28. Extracting the information from time-resolved fluorescence spectra requires building a detailed functional compartmental model describing the processes that affect the observed fluorescence of the photosystems in the thylakoid membrane.[29,30] At 77 K more details on the different emissive species can be distinguished, in particular of species with red-shifted emission relative to that of the RC. In an earlier paper[31] measurements of native and unstacked thylakoid membranes from spinach and their constituents were globally analyzed. The lifetimes and their decay associated spectra (DAS) were estimated and qualitatively interpreted. The aim of this paper is to build a more detailed target model (explained in detail in the Methods section) and extract the energy transfer pathways and decay characteristics of the different emissive species. By combining kinetic schemes with different spectral constraints we estimate the species associated spectra (SAS) and the microscopic rate constants of the energy transfer pathways and decays. In particular, introduction of spectral constraints enables us to estimate the SAS and free energy levels (relative to the bulk Chl a antenna) of the reaction center and of red Chl pools. This method is applied here to some of the units in the thylakoid membrane, for example, LHCI-PSI complexes, PSII membranes (BBY preparations),[31] and PSII core complexes.[26] A future aim is to obtain a quantitative description of functional changes in the thylakoid membrane upon regulatory processes like state transitions or nonphotochemical quenching.[32] As a case study, here a quantitative model is proposed that supports the formation of LHCII-LHCI-PSI supercomplexes in the transition from native to unstacked thylakoid membranes, as suggested before.[31]

MATERIALS AND METHODS

Samples, treatments, and measurement protocols have been described in detail before in refs 26 and 31. Briefly, time-resolved fluorescence spectra at 77 K were recorded of (1) PSI-LHCI complexes isolated from spinach thylakoid membranes, (2) PSII core complexes isolated from *Thermosynechococcus elongatus*, (3) PSII membranes (BBY preparations) isolated from spinach thylakoid membranes, and (4) native and unstacked spinach thylakoid membranes. The data from samples 1, 3, and 4 were obtained from ref 31, and those from sample 2 were obtained from ref 26. All data were previously measured at 77 K using a Synchroscan streak-camera setup, described in detail in ref 33 using an excitation wavelength of ≈485 nm, thus preferentially exciting Chl b

Special Issue: Rienk van Grondelle Festschrift

Received: March 29, 2013
Revised: July 12, 2013

   dx.doi.org/10.1021/jp4031283 | *J. Phys. Chem. B* XXXX, XXX, XXX−XXX

and carotenoids, for all samples except for the PSII core complexes where instead a nonselective 400 nm excitation wavelength was used. The repetition rate of the laser was 50 kHz with a pulse energy of 20 nJ (10 nJ for the PSII core complex) and a spot diameter of 1 mm. Spectra were recorded over a spectral width of approximately 250 nm with resolution of 2−4 nm over a total time range of 800 ps or 2 ns. The full width at half-maximum (fwhm) of the instrument response function (IRF) of the system was determined to be ≈10 ps for the 800 ps time range and ≈25 ps for the 2 ns time range.

The data reported in this paper were analyzed using a combination of global and target analysis.[29,30,34] Global analysis provides a simple description of the data at all wavelengths and all time points simultaneously, hence the word **global**. The simplest description of the data uses a number of independent exponentially decaying components, each represented by a single rate constant (reciprocal of the lifetime) and an amplitude at each recorded wavelength, together constituting the decay associated spectra (DAS). The DAS reflect the rise and decay of the components with their corresponding lifetimes. A sequential model estimates the same lifetimes and is easily written as a linear combination of the DAS but instead describes the spectral evolution of the data. The first compartment is excited and decays with the first lifetime into the second compartment. In turn, the second compartment decays into the third compartment, and so forth. The emission of each compartment is now described by an evolution associated spectrum (EAS). Target analysis combines the parallel and sequential aspects from global analysis into a full kinetic model which specifies the microscopic rate constants that describe the decay of each of the compartments as well as the energy transfer between compartments; as a result also equilibria between different compartments can be estimated. The emission of each compartment is now described by a species associated spectrum (SAS). In general, the number of free kinetic parameters is larger than the number of lifetimes estimated in global analysis. Therefore spectral constraints are needed, which limit the number of spectral parameters, and enable the estimation of additional kinetic parameters. Four types of spectral constraints can be distinguished, three of which apply to a particular wavelength region: zero constraints, nonnegativity constraints, and spectral relations.[29,35] The fourth type of spectral constraint considers the area of the complete SAS, which represents the oscillator strength of the emissive species. When the ratio between the oscillator strengths of two Chl species with SAS_i and SAS_j is assumed to be α, then a penalty can be imposed which is added to the least-squares criterion of the fit:

$$\text{penalty}_{ij} = \text{weight}_{ij} \int_{\lambda\text{min}}^{\lambda\text{max}} |\text{SAS}_i(\lambda) - \alpha \text{SAS}_j(\lambda)| \text{d}\lambda$$

Without a priori knowledge, we assume that all Chl species possess the same oscillator strength, that is, $\alpha = 1$. Here weight_{ij} is used to tune the importance of this area constraint in the least-squares fitting process. In practice, one starts with a small weight_{ij}, which is manually increased in subsequent fits. This penalty automates the trial and error approach that was used before.[5]

The aim of our target analysis is to construct functional compartmental models. In such a model we aim for a minimal number of compartments that describe the complete spectral evolution of the emission. Each compartment contains one or more pigments with the same spectrum and functional role. The basic model consists of an antenna compartment in equilibrium with one or more Red Chl pools and a reaction center (RC) compartment from which charge separation can occur (see Figure 1). The Red Chl pools absorb to the red of

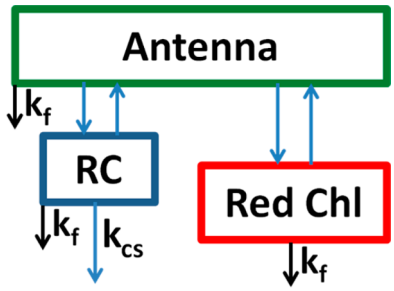

Figure 1. Functional compartmental model describing photosystem dynamics.

the RC, and they are pronouncedly present as slow decay components in the time-resolved emission, in particular at low temperature. They decay both via the bulk antenna (possibly followed by charge separation in the RC) and via their natural lifetime ($1/k_f$), which is assumed to be the same for all excited states. The free energy difference between two compartments depends upon the energy difference between the two emission maxima and upon the relative number of pigments of the compartments ($k_B T \ln(N_1/N_2)$).

Even when we assume k_f known (typically 1/(5 ns)), the model of Figure 1 contains five unknown microscopic rate constants. The three emissive compartments will yield three lifetimes, which means that we still require two constraints. Assuming equal areas of the three SAS provides us with these two constraints and enables estimation of all unknown kinetic parameters. Thus we resolve each equilibrium and determine the free energy differences between the three states.

RESULTS AND DISCUSSION

LHCI-PSI. The LHCI-PSI time-resolved fluorescence data was first analyzed by means of global analysis using a model with a minimal number of exponentials. Five components, as used in the original analysis, were found to already adequately fit the data.[31] However, using a sixth component, restricted to only contribute to the emission below 680 nm, was found to further improve the rms error of the fit by 1% with respect to five components and to account for some of the subps evolution in the emission on the blue side of the spectrum. The results of this analysis are summarized in Figure S1C in the form of the DAS and their corresponding lifetimes. The first DAS can be interpreted as the ultrafast energy transfer processes from Chl b to Chl a and from more blue Chl a to more red Chl a. Further equilibration, evidenced by negative DAS amplitudes, takes place on time scales of 11 and 40 ps. Trapping, evidenced by the net loss of DAS area, occurs on multiple time scales (11 and 40 ps, 0.42 and 1.9 ns). The last lifetime of ≈4.5 ns corresponds to a mixture of free LHC emitting at ≈675 nm, and a pigment emitting at ≈740 nm, from which excitations cannot escape to the RC via the bulk antenna.

Based on these observations a target model can be constructed. We know that at least six exponentials will be needed, but that possibly more components can be estimated. For instance, in a target model the 4.5 ns DAS, which consists

dx.doi.org/10.1021/jp4031283 | J. Phys. Chem. B XXXX, XXX, XXX−XXX

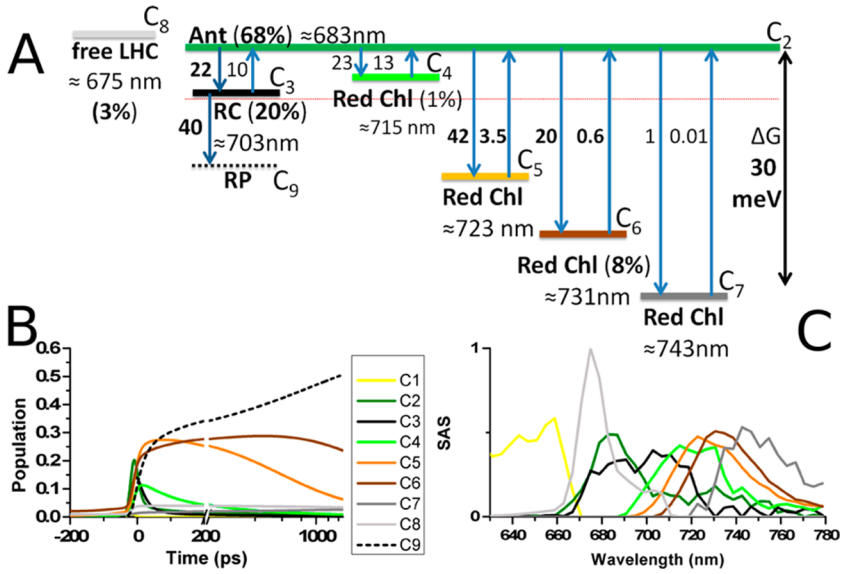

Figure 2. (A) Compartmental model used for target analysis of LHCI-PSI. Compartment C_1 as well as the k_{fl} rate constant for excited states have been omitted for clarity. The (x%) reflects the population after decay of C_1. Estimated microscopic rate constants (to the left of each arrow) are in 1/(ns). Bold numbers indicate relative precision better than 20%. The free energy scale is indicated; the thin red line represents k_BT = 6.6 meV below C_2. (B) Population profiles. (C) Corresponding estimated SAS.

of two functionally different species, can be split into two components with the help of zero constraints on the SAS. Furthermore from these results, it is obvious that several Red Chl pools in equilibrium with the RC via a bulk compartment will be needed. The equal area constraints on the SAS described in Materials and Methods allow us to estimate those equilibria.

The kinetic scheme of the target model is depicted in Figure 2A. Compartment C_1, a precursor to the other compartments, as well as the k_{fl} rate constant have been omitted from this figure for clarity. The characteristics of the different compartments of the target are collated in Table S1. The resulting population profiles and corresponding SAS that then describe the data are given in Figure 2B and C, respectively. The main idea behind this model is that most of the energy is very quickly distributed among all the pigments, partly via direct excitation (transfer from directly excited Chl b and Car) and partly via the antenna/bulk pigments. The excitation energy is then trapped at different time scales due to the equilibria between states of lower free energy and the bulk compartment which is in equilibrium with the RC.

The second compartment in the target model (C_2, depicted in dark green) captures a relatively short-lived species emitting at 683 nm, consistent with the emission of bulk Chl a. Bulk Chl a is modeled to be in direct equilibrium with the RC and with several Red Chl pool compartments as per Figure 1. The third compartment (C_3, depicted in black) is the RC compartment, with an emission peaking around 683 and 703 nm. The RC compartment decays via charge separation ("trapping") with rate k_{CS}. Several pools of Red Chl are connected to the bulk antenna, in total four distinct pools can be resolved. The fourth compartment represents a Red Chl pool (C_4, depicted in green) which peaks around 715 nm, and excitations trapped here have a relatively high probability to escape, explaining its observed lifetime of ≈96 ps. Recently, we resolved a very similar Chl a pool also in a PSI core preparation "without red Chl".[36] The free energy of the fifth compartment (C_5 depicted in orange), emitting around 723 nm, is slightly lower, resulting also in a longer lifetime of 0.5 ns. The sixth compartment (C_6 depicted in brown), is a very low lying state with respect to the RC and features a large emission band around 730 nm, characteristic for LHCI. This compartment is directly populated from the precursor, indicating that it is a red trap in LHCI, and it decays in 2.1 ns. Finally the seventh compartment (C_7, indicated by dark gray) represents a pool of Chl from which it is practically impossible to escape, resulting in a long ≈4 ns lifetime, probably representing the fraction of most red traps present in the inhomogeneous distribution of energy states in LHCI.

The estimated equilibria for this model are collated in Table S2. At 77 K the available thermal energy k_BT is about 6.6 meV or 54/cm, corresponding to a shift of 2.6 nm near 700 nm. The free energies of C_5, C_6, and C_7 are more than $2k_BT$ below that of the RC compartment C_3. This results in delayed trapping times in PSI at 77 K. To confirm that it is indeed possible to escape from a red trap, let us assume that the ratio of the number of pigments of the C_2 and C_5 compartments N_{C_2}/N_{C_5} is 100. Then the entropic free energy difference equals k_BT ln(100) = $4.6k_BT$ = 31 meV. We observe that $\Delta G_{C_2C_5}$ = 16 meV, which means that the energy difference between a C_2 Chl a and a C_5 red Chl a equals 47 meV or 371/cm equivalent to 703 nm (relative to 685 nm). With red Chl SAS the 0−0 transition is located at the blue edge of the SAS.[13] Thus it is possible that an excitation trapped in C_5 can escape to the RC, resulting in a 0.5 ns lifetime. Analogously, assuming N_{C_2}/N_{C_6} = 200, and observing $\Delta G_{C_2C_6}$ = 24 meV the energy difference between a C_2 Chl a and a C_6 red Chl a equals 59 meV or 476/cm equivalent to 708 nm (relative to 685 nm). Consequently, an excitation in C_6 where the blue edge of the SAS is ≈8 nm more red-shifted than that of C_5 can escape in 2.1 ns.

The estimated global lifetimes in this target analysis are 0.3 ps, 9 ps, 21 ps, 96 ps, 0.5 ns, 2.1 ns, 3.9 ns, and 4.1 ns. The amplitude matrix, Table S1, indicates that the fastest trapping (dashed black line in Figure 2B) occurs in 21 ps, whereas the ≈96 ps and 0.5 ns time scales correspond to escape from C_4

dx.doi.org/10.1021/jp4031283 | J. Phys. Chem. B XXXX, XXX, XXX−XXX

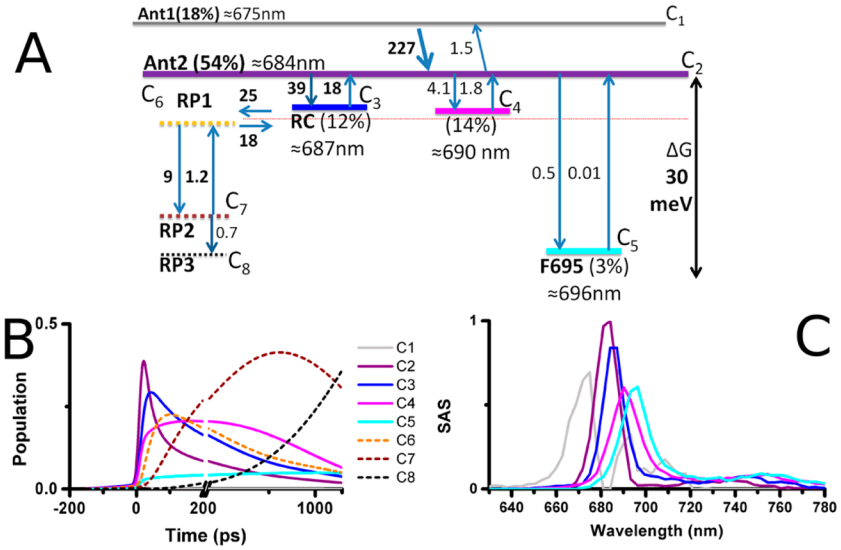

Figure 3. (A) Compartmental model used for target analysis of PSII core. The k_{fl} rate constant for excited states has been omitted for clarity. The (x %) reflects the initial population. Estimated microscopic rate constants (to the left of each arrow) are in 1/(ns). Bold numbers indicate relative precision better than 20%. The free energy scale is indicated; the thin red line represents k_BT = 6.6 meV below C_2. (B) Population profiles. (C) Corresponding estimated SAS.

and C_5 via the bulk C_2. The 9 ps lifetime represents equilibration of the excitation among the various pigments pools. The largest rises of the radical pair compartment are with 21 ps, 2.1 ns, and 0.5 ns, respectively, with a total yield of photochemical quenching of almost 66%. Of these 66%, already 34% occur on the 21 ps time scale.

The quality of the fit for this target analysis is good, as can be seen from the traces with all data and fits in Figure S2. All SAS shapes are realistic, except for the yellow one. The most interesting SAS here is the reaction center compartment C_3 (black in Figure 2C). It is bimodal with bands around 703 and 683 nm. We interpret these as the combined emission from P700 and the other chlorins of the RC and probably also some bulk Chl a in the core. Recently, in a target analysis of room temperature LHCI-PSI time-resolved fluorescence data,[12] four compartments could be resolved, two of which were red Chl pools in the core and the antenna. The 77 K data thus allow resolving two more red Chl pools. At room temperature two separate compartments (with identical SAS) were resolved for the bulk Chl a in the core, and in LHCI. Here we can describe the 77 K data with a single bulk Chl a compartment, which is an oversimplification.

PSII Core Complexes. The time-resolved emission of PSII cores of *Thermosynechococcus elongatus* was recorded at 77 K upon 400 nm excitation.[26] Inspired by the success of the LHCI-PSI target analysis (see above) we revisited these 77 K data, using an analogous model with traps in equilibrium with bulk Chl a. Note that here again the area constraint explained above was crucial to extract more information from the data. In global analysis five exponentials were necessary to describe the data. The DAS in Figure S1A are more congested than of PSI-LHCI in Figure S1C, because there are less red chlorophylls in PSII than in PSI. Equilibration in ≈7 ps is present. Trapping occurs on multiple time scales (27 and ≈158 ps, ≈0.9 ns). The last lifetime of ≈4.3 ns corresponds to a pigment emitting at ≈696 nm.

For the target analysis, we used the kinetic scheme depicted in Figure 3A. The characteristics of the different compartments of this model are collated in Table S3, while the resulting population profiles and corresponding SAS that describe the data are given in Figure 3B and C, respectively. The first two compartments in this model (C_1, gray SAS and C_2, purple SAS) represent antenna pools Ant1 and Ant2 emitting at ≈675 and ≈684 nm. They equilibrate in ≈4 ps, consistent with pump probe results at 77 K in CP43 and CP47 showing main energy transfer times of ≈0.3 and ≈3 ps in both core antenna complexes.[37] In the target model we assumed furthermore that Ant2 (C_2) is in equilibrium with the RC compartment C_3 (blue SAS) emitting at ≈687 nm. C_3 is in fast equilibrium with a dark RP1 state (C_6), in agreement with several results on charge separation in PSII.[19,26,38,39] RP1 (C_6, orange population profile, no SAS) in turn is in equilibrium with the dark state RP2 (C_7, brown population profile, no SAS), although the back reaction is small. In addition, the bulk antenna pool C_2 is in equilibrium with two red Chl a pools C_4 and C_5 from CP47[40−42] emitting at ≈690 and ≈696 nm with lifetimes of about 0.58/1.8 and 4 ns, respectively. To verify that C_4 can still escape via the antenna to the RC, we can again make an assumption for the relative number of pigments in the core compartment (C_2) and the red trap C_4 and calculate the free energy difference. For PSII a reasonable estimate for N_{C_2}/N_{C_4} is 30. Then the entropic free energy difference equals $k_BT \ln(N_{C_2}/N_{C_4}) = 3.4k_BT$ = 23 meV. We observe that $\Delta G_{C_2,C_4}$ = 6 meV, which means that the energy difference between a C_2 Chl a and a C_4 red Chl a equals 29 meV or 234/cm, equivalent to 691 nm (relative to 680 nm). Thus it is possible that an excitation trapped in C_4 can escape to the RC, resulting in a 0.58/1.8 ns lifetime.

From the amplitude matrix, Table S3, we read that the main decay times of the bulk (C_2) antenna are 13.5 and 29 ps, concomitant with the rises of RC and RP1 on these time scales. The red pigment emitting at ≈690 nm (C4, black spectrum in Figure 3C) decays with 0.58 and 1.8 ns. Trapping (dashed orange, brown, and black lines in Figure 3B) is predominantly occurring with 164 ps and 0.58 ns, as evidenced from the largest rises of the RP2 compartment, with a total yield of photochemical quenching of 77%. The remaining 23% decays to the ground state mainly through the two red Chl pools.

dx.doi.org/10.1021/jp4031283 | J. Phys. Chem. B XXXX, XXX, XXX−XXX

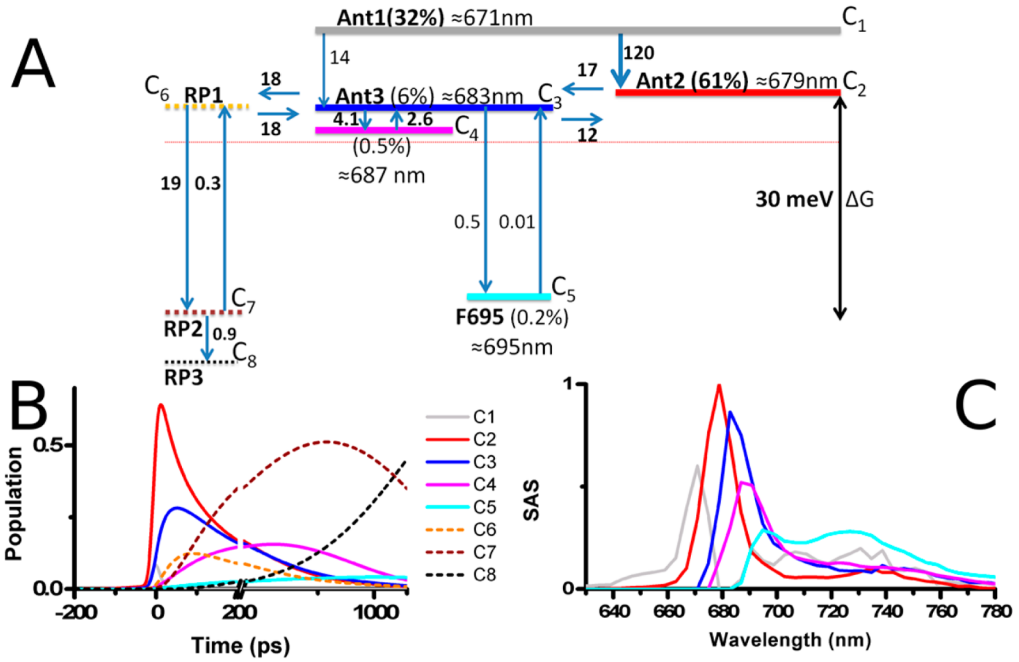

Figure 4. (A) Compartmental model used for target analysis of PSII membranes. The k_{fl} rate constant for excited states have been omitted for clarity. Estimated microscopic rate constants (to the left of each arrow) are in 1/(ns). Bold numbers indicate relative precision better than 20%. The free energy scale is indicated; the thin red line represents k_BT = 6.6 meV below C_2. (B) Population profiles. (C) Corresponding estimated SAS.

The quality of the fit for this target analysis is good; see the traces with all data and fits in Figure S3. All SAS shapes are realistic, with the shortest living gray SAS being estimated less precisely.

PSII Membranes. PSII membranes contain PSII cores connected with a large outer antennae.[43] The excitation wavelength for the PSII membranes was 485 nm, rather than the 400 nm for PSII core, thus again exciting preferentially Chl b, which is present in LHCII and the minor antenna complexes CP29, CP26, and CP24.[3] In global analysis five exponentials were found to be necessary to describe the data (Figure S1B). Similar to PSII core, interantenna equilibration in ≈8 ps is present. The 44 ps DAS is almost conservative, attributed to further equilibration, possibly between peripheral and core antennae. Trapping time scales are ≈139 ps and ≈0.53 ns.

For the target analysis we started from the same kinetic scheme as with the PSII core (Figure 4A). The Ant1 compartment (C1) now contains blue Chl a and Chl b. The Ant2 compartment represents the bulk Chl a of the peripheral antennae. With the 485 nm excitation, we could no longer reliably resolve an RC compartment, which is now included in the Ant3 compartment that is dominated by the bulk Chl a of core antenna complexes CP43 and CP47. The characteristics of the different compartments of the target model used to analyze the PSII membrane data are collated in Table S5. The resulting population profiles and corresponding SAS that then describe the data are given in Figure 4B and C, respectively. The quality of the fit for this target analysis is good; see the traces with all data and fits in Figure S4. We attempted to add an RC compartment, but this did not improve the quality of the fit.

The estimated SAS of PSII membranes are similar to those of PSII core, with the obvious exception that Ant1 (C1, gray SAS) now contains a Chl b contribution. The parameters estimated with the PSII core complexes and the PSII membrane data are somewhat different. In the membranes, the equilibration is slower, in particular because of the equilibration between peripheral C_2 and core C_3 antennae. The estimated equilibria for this model are collated in Table S6. The free energy of C_4 is only 3 meV below that of C_3, enabling escape from the 687 nm chlorophyll (C_4) to C_3 which includes the RC. The 695 nm chlorophyll (C_5) lies more than 4 times kT below C_3. Especially from the long-lived species (C_5, cyan SAS in Figure 4C) it is clear that this particular sample was contaminated with PSI-LHCI, resulting in an increased amplitude around 730 nm.

From the amplitude matrix, Table S5, we read that the main decay times of the C_2 bulk antenna are 37 and 144 ps, concomitant with the rises of Ant3 and RP1 on these time scales. The pigments emitting at 687 nm (C_4, magenta spectrum in Figure 4C) decay with 0.52 ns. Trapping (dashed orange, brown, and black lines in Figure 4B) is visible in the largest rises of the RP2 compartment with 144 ps and 0.52 ns, with a total yield of photochemical quenching of 84%. The remaining 16% decays to the ground state mainly through the two red Chl pools. Note that the main difference in the trapping compared to Figure 3B is the delayed and smaller population of RP1 (orange).

Native and Unstacked Thylakoid Membranes. The DAS depicted in Figure S1D and E for native and unstacked membranes both contain five lifetimes: a fast energy transfer of 11 ps, trapping on time scales of ≈38 ps, ≈150 ps, and ≈0.6 ns. The final decay is in ≈3 ns. From the shapes of the DAS, in particular the larger contribution of red emission from PSI in Figure S1E, a transition is already apparent.[31] We recognize here the trapping time scales that we have seen before for either PSI or PSII. There we learned that we can resolve up to eight compartments for PSI-LHCI and seven for PSII membranes. All of these SAS overlap, and in measurements on whole stacked and unstacked thylakoid membrane they all come together. However, given the limited signal-to-noise ratio of the data used in this study it is not possible to resolve 15 functional compartments in a model for the emission from a complete

dx.doi.org/10.1021/jp4031283 | J. Phys. Chem. B XXXX, XXX, XXX−XXX

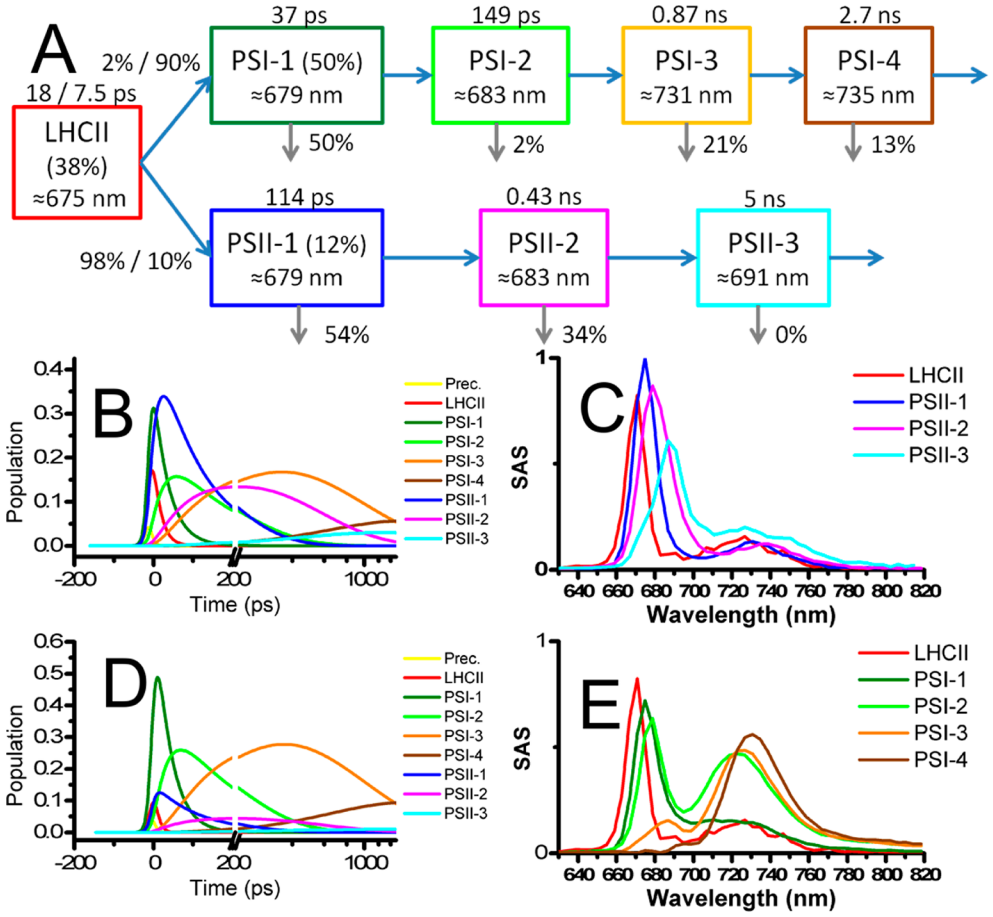

Figure 5. (A) Compartmental model used for the simultaneous target analysis of the stacked and unstacked thylakoid membranes. Note that the model allows for a different rate of energy transfer from the LHCII compartments between data sets. Numbers at the errors are rates in 1/ns; downward arrows represent photochemical quenching. Compartment C_1 as well as the k_{fl} rate constant for excited states have been omitted for clarity. (B) Population profiles for the stacked thylakoid membrane and (C) estimated LHCII and PSII SAS. (D) Population profiles for unstacked thylakoid membrane and (E) estimated LHCII and PSI SAS.

thylakoid membrane. Therefore we set out for a limited target model, with which we describe *simultaneously* the native and unstacked thylakoid membrane. We model each photosystem with a sequential scheme with four compartments for PSI and three compartments for PSII. The area constraint of the subsequent SAS was used here to quantify the amount of trapping at each step. Each initial photosystem compartment can be directly excited, and it receives input from the LHCII antenna. The native and unstacked thylakoid membrane mimic a state transition. In our target analysis the aim is to quantify this transition, by estimating the amount of input that each initial photosystem compartment receives from the LHCII antenna in each state. Thus the simultaneous target analysis of emission data from two states is instrumental to resolve the distribution of energy in these states.

The characteristics of the different compartments of the target model used to analyze the stacked-unstacked thylakoid data are indicated in Figure 5A together with the kinetic scheme. The resulting population profiles that then describe the data are given in Figure 5B and D for the native and unstacked membranes, respectively. The corresponding SAS of PSII and PSI are depicted in Figure 5C and E, respectively. These SAS are not pure, since they contain contributions from red Chl pigments and from bulk antennae (especially for PSI).

The estimated lifetimes in the stacked/unstacked case respectively are 1 ps, 18 ps/7.5 ps (for LHCII), 37 ps, 114 ps, 149 ps, 429 ps, 873 ps, 2.7 ns, and 5.0 ns. The amplitude matrices for the stacked and unstacked case are reported separately in Tables S7 and S8, respectively. The rise of the stable charge separated state of PSI (RP PSI) indicates that the fastest PSI trapping occurs in 37 ps, with minor contributions in 0.9 and 2.7 ns. The rise of the stable charge separated state of PSII (RP PSII) occurs on time scales of 114 and 429 ps.

The quality of the fit for this target analysis is good; see the traces with all data and fits in Figure S5.

Although we resolve less compartments for PSI and PSII, an LHCII SAS is resolved. It peaks at 675 nm, to the blue of the core antennae (red SAS in Figure 5C,E). Its lifetime is shorter, and its peak is blue-shifted compared to the LHCII SAS resolved with BBY membranes (cf. the red SAS in Figure 4C). This is caused by the unidirectionality of the energy transfer from LHCII in this oversimplified model. Because of the small weight used, the penalty amounts to an increase of the rms error of the fit by 0.3%. This allows for a 2-fold area difference between the smallest and largest SAS area. We chose not to increase the weight, since there are already other shortcomings of this model (most importantly the missing equilibria).

dx.doi.org/10.1021/jp4031283 | J. Phys. Chem. B XXXX, XXX, XXX−XXX

The amount of direct excitation of LHCII, PSI-LHCI, and PSII was estimated to be about 38%, 50%, and 12% in stacked and unstacked conditions. These numbers are reasonable in view of the 485 nm excitation wavelength and the amount of Chl b and carotenoids in the three systems.

The relative estimated amount of LHCII that transferred to PSII and PSI in stacked and unstacked conditions is collated in Table 1. The transition is almost complete, with the input to PSII decreasing from 98 to 10%, concomitant with the input to PSI increasing from 2 to 90%.

Table 1. Energy Transfer Rates (in 1/ns) from the LHCII Compartment to PSI and PSII in Stacked and Unstacked Conditions[a]

	PSII	PSI
stacked	54 (98%)	1 (2%)
unstacked	14 (10%)	121 (90%)

[a]The parentheses indicate the fractions of LHCII transferring to PSI and PSII.

Reconstruction of the Steady-State Fluorescence Spectra. The target models obtained allow reconstruction of the steady state fluorescence spectra. These are shown in Figure S6. Taking into account the lower wavelength resolution of ≈3 nm, they generally agree with measured steady state fluorescence spectra. In addition, these reconstructions provide useful insight into the origins of the constituent bands. With LHCI-PSI the reconstructed steady state emission in Figure S6C is dominated by the contributions of the 730 nm SAS (C_6, brown) and 675 nm free LHC SAS (C_8, gray). In addition, the 723 and 743 nm SAS (C_5, orange and C_7, dark gray) contribute.

With PSII cores (Figure S6A) the dominant contributions are the 687, 690, and 696 nm SAS (blue, magenta, and cyan) which represent the RC and the two red Chl pools. In this model, the well-known F695 emission of PSII at 77 K originates from C_5 peaking at 696 nm, while F685 represents the combined contributions of C_2 (the bulk antenna chlorophylls emitting at 684 nm), C_3 (the RC chlorophylls and pheophytins), and C_4 (the red chlorophyll of CP47 that emits at 690 nm and transfers its energy to the RC with a lifetime of 0.58/1.8 ns at 77 K).

In BBY membranes (Figure S6B), the contribution of peripheral antenna C_2 is larger than in PSII core, where C_2 represented core antenna. The large contribution of the cyan SAS around 730 nm results from the above-mentioned contamination with PSI-LHCI.

In the case of stacked and unstacked thylakoid membranes, cf. Figure S6D and E, we observe that after the transition the PSII bands decrease and that half of the remaining emission at 685 nm is attributable to PSI Chl a.

Uniqueness of the Models. The number of parameters that we estimate is larger than before,[26] in particular because we estimate here all equilibria. The information to estimate these equilibria is derived from the equal SAS area constraint. In LHCI-PSI (Figure 2) we resolved eight well-separated SAS, and the relative precision of most microscopic rate constants was 20% or better. Although in PSII core the SAS are more congested, two red Chl contributions are well-resolved. The relatively slow equilibration of CP43 and CP47 antenna and RC is consistent with the computations of Renger et al.[44,45] The BBY target analysis was consistent with that of PSII core, and the differences in the dynamics and energetics were explainable by the equilibration with the outer antenna. More information is needed to test the models proposed here, for example, from further studies using data measured with different excitation wavelengths, at multiple temperatures[46] or at other different measurement conditions.[47] In particular, to more completely functionally characterize the whole thylakoid membrane, simultaneous analysis of multiple experiments will be needed. In addition to the equal SAS area constraint, other penalties based upon SAS shape could be useful to decide between alternative models, for example, smoothness.[48]

CONCLUSIONS

We modeled the dynamics of PSI and PSII at 77 K using a kinetic scheme where red pigment pools are in equilibrium with the RC via the bulk antenna. Excitation energy can then either be trapped directly by the RC via downhill energy transfer processes or depending on the free energy difference between the red pigment pool and the intermediate compartment also by escaping to the RC via the bulk antenna, resulting in the observed trapping on various time scales.

In the target analysis spectral constraints, in particular SAS of equal area and non-negativity of the SAS, were essential for the estimation of all relevant parameters from the data. We have demonstrated that this type of model generally works for all photosystems, specifically for LHCI-PSI from spinach, PSII core complexes of *Thermosynechococcus elongatus*, and PSII membranes from spinach. For the first time we have been able to resolve the SAS of the RC of PSII, which possesses a single maximum at ≈684 nm.

We have also shown that the dynamics of a system as complex as a whole thylakoid membrane, containing LHCI-II, LHCI-PSI, and PSII, can be modeled using a relatively simple scheme in which the difference in the emission between two states of the same system (in this case stacked and unstacked thylakoid membranes) is used to resolve the photosystem dynamics to a large degree. Specifically in the case of stacked and unstacked thylakoid membranes it allowed the quantification of the amount of LHCII involved in the process. In the model, the LHCII input to PSII decreased from 98 to 10%, whereas the input to PSI increased from 2 to 90%. This means that in stacked membranes, almost all LHCII transfers its excitation energy to PSII, in agreement with the physical separation of LHCII and PSII in the grana and of PSI in the stroma membranes. After unstacking, PSII, PSI, and LHCII are fully mixed in one membrane system, and now the majority of LHCII transfers its energy to PSI.

These results indicate that time-resolved emission followed by a target analysis can be used to quantify a sample in terms of functional connectivity of the peripheral light-harvesting antenna and each of the two photosystems.

ASSOCIATED CONTENT

Supporting Information

Six figures showing DAS, all data and fits, and reconstructed steady state spectra. Eight tables detailing the amplitude matrices of the compartmental models and free energy differences. This material is available free of charge via the Internet at http://pubs.acs.org.

AUTHOR INFORMATION

Corresponding Author

*E-mail: i.h.m.van.stokkum@vu.nl.

dx.doi.org/10.1021/jp4031283 | J. Phys. Chem. B XXXX, XXX, XXX−XXX

Notes

The authors declare no competing financial interest.

■ ACKNOWLEDGMENTS

This project was carried out in part within the research programme of BioSolar Cells, cofinanced by the Dutch Ministry of Economic Affairs (J.J.S., J.D., R.v.G., and I.H.M.v.S.). R.v.G. and I.H.M.v.S. acknowledge financial support of the European Research Council (Advanced Grant proposal 267333 (PHOTPROT) to R.v.G.). We thank Roberta Croce, Bart van Oort, and Gert van der Zwan for a critical reading of the text or helpful discussion.

■ ABBREVIATIONS

Chl, chlorophyll; DAS, decay associated spectrum; EAS, evolution associated spectrum; GS, ground state; PSI, photosystem I; PSII, photosystem II; RC, reaction center; RP, radical pair; SAS, species associated spectrum

■ REFERENCES

(1) Holzwarth, A. R. Time-Resolved Fluorescence Spectroscopy. *Biochem. Spectrosc.* **1995**, *246*, 334−362.

(2) van Grondelle, R.; Dekker, J. P.; Gillbro, T.; Sundström, V. Energy-Transfer and Trapping in Photosynthesis. *Biochim. Biophys. Acta* **1994**, *1187* (1), 1−65.

(3) Croce, R.; van Amerongen, H. Light-Harvesting and Structural Organization of Photosystem II: From Individual Complexes to Thylakoid Membrane. *J. Photochem. Photobiol., B* **2011**, *104* (1−2), 142−153.

(4) Hastings, G.; Kleinherenbrink, F. A. M.; Lin, S.; Blankenship, R. E. Time-Resolved Fluorescence and Absorption-Spectroscopy of Photosystem-I. *Biochemistry* **1994**, *33* (11), 3185−3192.

(5) Gobets, B.; van Stokkum, I. H. M.; Rogner, M.; Kruip, J.; Schlodder, E.; Karapetyan, N. V.; Dekker, J. P.; van Grondelle, R. Time-Resolved Fluorescence Emission Measurements of Photosystem I Particles of Various Cyanobacteria: A Unified Compartmental Model. *Biophys. J.* **2001**, *81* (1), 407−424.

(6) Ihalainen, J. A.; Klimmek, F.; Ganeteg, U.; van Stokkum, I. H. M.; van Grondelle, R.; Jansson, S.; Dekker, J. P. Excitation Energy Trapping in Photosystem I Complexes Depleted in Lhca1 and Lhca4. *FEBS Lett.* **2005**, *579* (21), 4787−4791.

(7) Ihalainen, J. A.; van Stokkum, I. H. M.; Gibasiewicz, K.; Germano, M.; van Grondelle, R.; Dekker, J. P. Kinetics of Excitation Trapping in Intact Photosystem I of Chlamydomonas Reinhardtii and Arabidopsis Thaliana. *Biochim. Biophys. Acta—Bioenergetics* **2005**, *1706* (3), 267−275.

(8) Slavov, C.; Ballottari, M.; Morosinotto, T.; Bassi, R.; Holzwarth, A. R. Trap-Limited Charge Separation Kinetics in Higher Plant Photosystem I Complexes. *Biophys. J.* **2008**, *94* (9), 3601−3612.

(9) Shibata, Y.; Akai, S.; Kasahara, T.; Ikegami, I.; Itoh, S. Temperature-Dependent Energy Gap of the Primary Charge Separation in Photosystem I: Study of Delayed Fluorescence at 77−268 K. *J. Phys. Chem. B* **2008**, *112* (21), 6695−6702.

(10) Shibata, Y.; Yamagishi, A.; Kawamoto, S.; Noji, T.; Itoh, S. Kinetically Distinct Three Red Chlorophylls in Photosystem I of Thermosynechococcus Elongatus Revealed by Femtosecond Time-Resolved Fluorescence Spectroscopy at 15 K. *J. Phys. Chem. B* **2010**, *114* (8), 2954−2963.

(11) Melkozernov, A. N.; Kargul, J.; Lin, S.; Barber, J.; Blankenship, R. E. Energy Coupling in the PSI−LHCI Supercomplex from the Green Alga Chlamydomonas Reinhardtii. *J. Phys. Chem. B* **2004**, *108* (29), 10547−10555.

(12) Wientjes, E.; van Stokkum, I. H. M.; van Amerongen, H.; Croce, R. The Role of the Individual Lhcas in Photosystem I Excitation Energy Trapping. *Biophys. J.* **2011**, *101* (3), 745−754.

(13) Croce, R.; Chojnicka, A.; Morosinotto, T.; Ihalainen, J. A.; van Mourik, F.; Dekker, J. P.; Bassi, R.; van Grondelle, R. The Low-Energy Forms of Photosystem I Light-Harvesting Complexes: Spectroscopic Properties and Pigment-Pigment Interaction Characteristics. *Biophys. J.* **2007**, *93* (7), 2418−2428.

(14) Mozzo, M.; Mantelli, M.; Passarini, F.; Caffarri, S.; Croce, R.; Bassi, R. Functional Analysis of Photosystem I Light-Harvesting Complexes (Lhca) Gene Products of Chlamydomonas Reinhardtii. *Biochim. Biophys. Acta—Bioenergetics* **2010**, *1797* (2), 212−221.

(15) Romero, E.; Mozzo, M.; van Stokkum, I. H. M.; Dekker, J. P.; van Grondelle, R.; Croce, R. The Origin of the Low-Energy Form of Photosystem I Light-Harvesting Complex Lhca4: Mixing of the Lowest Exciton with a Charge-Transfer State. *Biophys. J.* **2009**, *96* (5), L35−L37.

(16) Jennings, R. C.; Zucchelli, G.; Engelmann, E.; Garlaschi, F. M. The Long-Wavelength Chlorophyll States of Plant LHCI at Room Temperature: A Comparison with PSI-LHCI. *Biophys. J.* **2004**, *87* (1), 488−497.

(17) Wientjes, E.; Croce, R. The Light-Harvesting Complexes of Higher-Plant Photosystem I: Lhca1/4 and Lhca2/3 Form Two Red-Emitting Heterodimers. *Biochem. J.* **2011**, *433*, 477−485.

(18) Barter, L. M. C.; Bianchietti, M.; Jeans, C.; Schilstra, M. J.; Hankamer, B.; Diner, B. A.; Barber, J.; Durrant, J. R.; Klug, D. R. Relationship between Excitation Energy Transfer, Trapping, and Antenna Size in Photosystem II. *Biochemistry* **2001**, *40* (13), 4026−4034.

(19) Miloslavina, Y.; Szczepaniak, M.; Muller, M. G.; Sander, J.; Nowaczyk, M.; Rogner, M.; Holzwarth, A. R. Charge Separation Kinetics in Intact Photosystem II Core Particles Is Trap-Limited. A Picosecond Fluorescence Study. *Biochemistry* **2006**, *45* (7), 2436−2442.

(20) Broess, K.; Trinkunas, G.; van der Weij-de Wit, C. D.; Dekker, J. P.; van Hoek, A.; van Amerongen, H. Excitation Energy Transfer and Charge Separation in Photosystem II Membranes Revisited. *Biophys. J.* **2006**, *91* (10), 3776−3786.

(21) van Oort, B.; Alberts, M.; de Bianchi, S.; Dall'Osto, L.; Bassi, R.; Trinkunas, G.; Croce, R.; van Amerongen, H. Effect of Antenna-Depletion in Photosystem II on Excitation Energy Transfer in Arabidopsis Thaliana. *Biophys. J.* **2010**, *98* (5), 922−931.

(22) Caffarri, S.; Broess, K.; Croce, R.; van Amerongen, H. Excitation Energy Transfer and Trapping in Higher Plant Photosystem II Complexes with Different Antenna Sizes. *Biophys. J.* **2011**, *100* (9), 2094−2103.

(23) Gatzen, G.; Muller, M. G.; Griebenow, K.; Holzwarth, A. R. Primary Processes and Structure of the Photosystem II Reaction Center. 3. Kinetic Analysis of Picosecond Energy Transfer and Charge Separation Processes in the D1-D2-Cyt-B559 Complex Measured by Time-Resolved Fluorescence. *J. Phys. Chem.* **1996**, *100* (17), 7269−7278.

(24) Roelofs, T. A.; Lee, C. H.; Holzwarth, A. R. Global Target Analysis of Picosecond Chlorophyll Fluorescence Kinetics from Pea-Chloroplasts - a New Approach to the Characterization of the Primary Processes in Photosystem-II Alpha-Units and Beta-Units. *Biophys. J.* **1992**, *61* (5), 1147−1163.

(25) Schatz, G. H.; Brock, H.; Holzwarth, A. R. Kinetic and Energetic Model for the Primary Processes in Photosystem-II. *Biophys. J.* **1988**, *54* (3), 397−405.

(26) van der Weij−de Wit, C. D.; Dekker, J. P.; van Grondelle, R.; van Stokkum, I. H. M. Charge Separation Is Virtually Irreversible in Photosystem II Core Complexes with Oxidized Primary Quinone Acceptor. *J. Phys. Chem. A* **2011**, *115* (16), 3947−3956.

(27) Broess, K.; Trinkunas, G.; van Hoek, A.; Croce, R.; van Amerongen, H. Determination of the Excitation Migration Time in Photosystem II - Consequences for the Membrane Organization and Charge Separation Parameters. *Biochim. Biophys. Acta—Bioenergetics* **2008**, *1777* (5), 404−409.

(28) Tian, L.; Farooq, S.; van Amerongen, H. Probing the Picosecond Kinetics of the Photosystem II Core Complex in Vivo. *Phys. Chem. Chem. Phys.* **2013**, *15* (9), 3146−3154.

(29) van Stokkum, I. H. M.; Larsen, D. S.; van Grondelle, R. Global and Target Analysis of Time-Resolved Spectra. *Biochim. Biophys. Acta* **2004**, *1657*, 82−104.
(30) Holzwarth, A. Data Analysis of Time-Resolved Measurements. In *Biophysical Techniques in Photosynthesis*; Amesz, J., Hoff, A., Eds.; Kluwer Academic Press: Dordrecht, 1996; pp 75−92.
(31) van der Weij-de Wit, C. D.; Ihalainen, J. A.; van Grondelle, R.; Dekker, J. P. Excitation Energy Transfer in Native and Unstacked Thylakoid Membranes Studied by Low Temperature and Ultrafast Fluorescence Spectroscopy. *Photosynth. Res.* **2007**, *93* (1−3), 173−182.
(32) Horton, P. Optimization of Light Harvesting and Photoprotection: Molecular Mechanisms and Physiological Consequences. *Philos. Trans. R. Soc. B, Biol. Sci.* **2012**, *367* (1608), 3455−3465.
(33) van Stokkum, I. H. M.; van Oort, B.; van Mourik, F.; Gobets, B.; van Amerongen, H. (Sub)-Picosecond Spectral Evolution of Fluorescence Studied with a Synchroscan Streak-Camera System and Target Analysis. In *Biophysical Techniques in Photosynthesis Vol. II*; Aartsma, T. J., Matysik, J., Eds.; Springer: Dordrecht, The Netherlands, 2008; pp 223−240.
(34) Snellenburg, J. J.; Laptenok, S. P.; Seger, R.; Mullen, K. M.; van Stokkum, I. H. M. Glotaran: A Java-Based Graphical User Interface for the R-Package Timp. *J. Stat. Software* **2012**, *49*, 1−22.
(35) Mullen, K. M.; van Stokkum, I. H. M. The Variable Projection Algorithm in Time-Resolved Spectroscopy, Microscopy and Mass Spectrometry Applications. *Numer. Algorithms* **2009**, *51* (3), 319−340.
(36) van Stokkum, I. H. M.; Desquilbet, T. E.; van der Weij−de Wit, C. D.; Snellenburg, J. J.; van Grondelle, R.; Thomas, J.-C.; Robert, B.; Dekker, J. P. Energy Transfer and Trapping in Red-Chlorophyll-Free Photosystem I from Synechococcus Wh 7803. *J. Phys. Chem. B* **2013**, 10.1021/jp401364a.
(37) de Weerd, F. L.; van Stokkum, I. H. M.; van Amerongen, H.; Dekker, J. P.; van Grondelle, R. Pathways for Energy Transfer in the Core Light-Harvesting Complexes Cp43 and Cp47 of Photosystem II. *Biophys. J.* **2002**, *82* (3), 1586−1597.
(38) Holzwarth, A. R.; Muller, M. G.; Reus, M.; Nowaczyk, M.; Sander, J.; Rogner, M. Kinetics and Mechanism of Electron Transfer in Intact Photosystem II and in the Isolated Reaction Center: Pheophytin Is the Primary Electron Acceptor. *Proc. Natl. Acad. Sci. U.S.A.* **2006**, *103* (18), 6895−6900.
(39) Groot, M. L.; Pawlowicz, N. P.; van Wilderen, L.; Breton, J.; van Stokkum, I. H. M.; van Grondelle, R. Initial Electron Donor and Acceptor in Isolated Photosystem II Reaction Centers Identified with Femtosecond Mid-Ir Spectroscopy. *Proc. Natl. Acad. Sci. U.S.A.* **2005**, *102* (37), 13087−13092.
(40) de Weerd, F. L.; Palacios, M. A.; Andrizhiyevskaya, E. G.; Dekker, J. P.; van Grondelle, R. Identifying the Lowest Electronic States of the Chlorophylls in the Cp47 Core Antenna Protein of Photosystem II. *Biochemistry* **2002**, *41* (51), 15224−15233.
(41) Vandorssen, R. J.; Breton, J.; Plijter, J. J.; Satoh, K.; Vangorkom, H. J.; Amesz, J. Spectroscopic Properties of the Reaction Center and of the 47kDa Chlorophyll Protein of Photosystem-II. *Biochim. Biophys. Acta* **1987**, *893* (2), 267−274.
(42) Komura, M.; Shibata, Y.; Itoh, S. A New Fluorescence Band F689 in Photosystem II Revealed by Picosecond Analysis at 4−77 K: Function of Two Terminal Energy Sinks F689 and F695 in PS II. *Biochim. Biophys. Acta—Bioenergetics* **2006**, *1757* (12), 1657−1668.
(43) Dekker, J. P.; Boekema, E. J. Supramolecular Organization of Thylakoid Membrane Proteins in Green Plants. *Biochim. Biophys. Acta—Bioenergetics* **2005**, *1706* (1−2), 12−39.
(44) Raszewski, G.; Renger, T. Light Harvesting in Photosystem II Core Complexes Is Limited by the Transfer to the Trap: Can the Core Complex Turn into a Photoprotective Mode? *J. Am. Chem. Soc.* **2008**, *130* (13), 4431−4446.
(45) Renger, T.; Schlodder, E. Primary Photophysical Processes in Photosystem II: Bridging the Gap between Crystal Structure and Optical Spectra. *ChemPhysChem* **2010**, *11* (6), 1141−1153.
(46) Nagle, J. F. Solving Complex Photocycle Kinetics—Theory and Direct Method. *Biophys. J.* **1991**, *59* (2), 476−487.
(47) van Stokkum, I. H. M.; Lozier, R. H. Target Analysis of the Bacteriorhodopsin Photocycle Using a Spectrotemporal Model. *J. Phys. Chem. B* **2002**, *106* (13), 3477−3485.
(48) de Juan, A.; Tauler, R. Multivariate Curve Resolution (MCR) from 2000: Progress in Concepts and Applications. *Crit. Rev. Anal. Chem.* **2006**, *36* (3−4), 163−176.

Functional Compartmental Modeling of the Photosystems in the Thylakoid Membrane at 77K

*Joris J. Snellenburg, Jan P. Dekker, Rienk van Grondelle, Ivo H.M. van Stokkum**

Institute for Lasers, Life and Biophotonics, Faculty of Sciences, VU University Amsterdam, De Boelelaan 1081, 1081 HV, Amsterdam, The Netherlands

Supporting information

Six figures showing DAS, all data and fits, and reconstructed steady state spectra. Eight tables detailing the amplitude matrices of the compartmental models, and free energy differences.

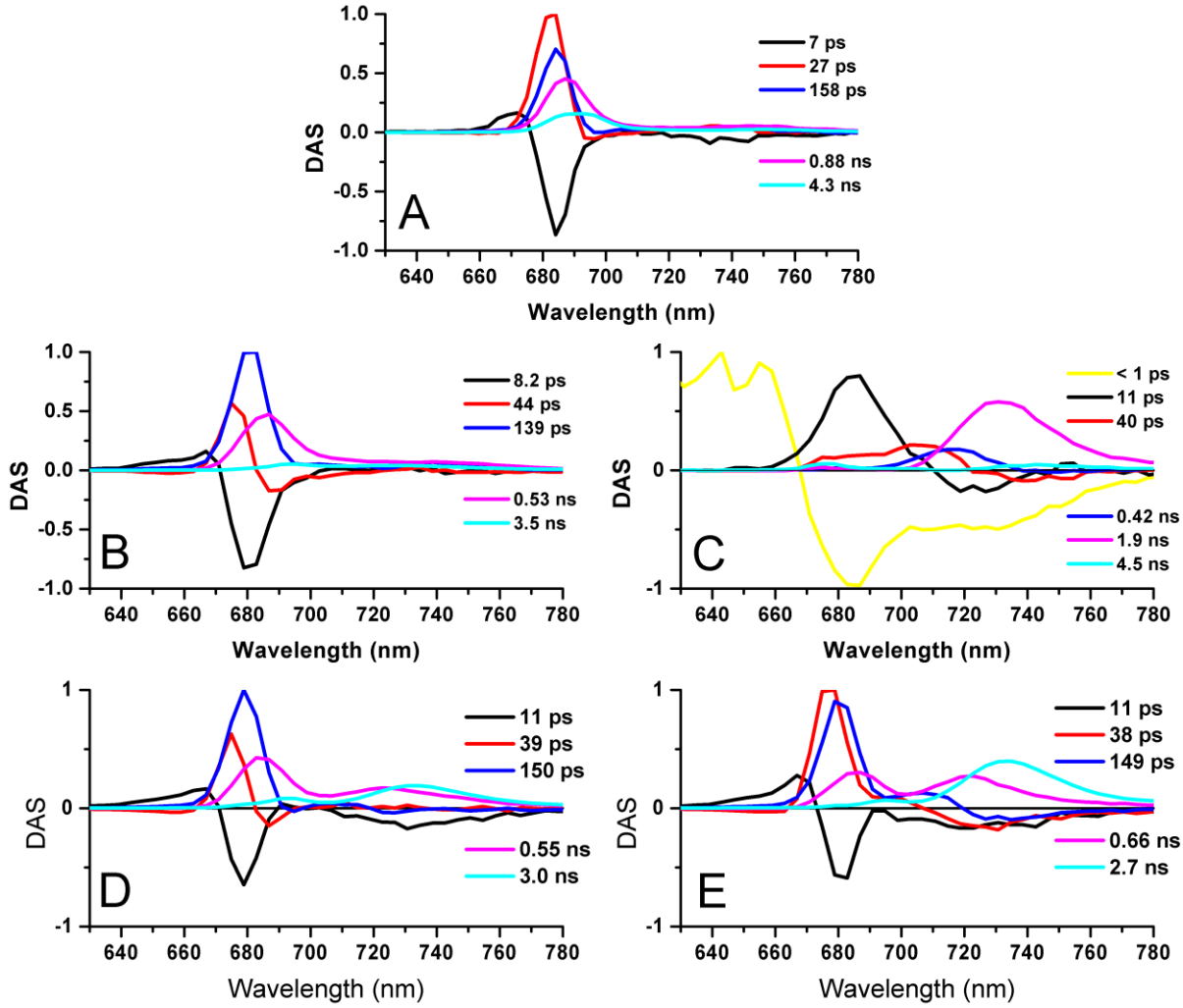

Figure S1. Estimated DAS resulting from global analysis using five (or six with LHCI-PSI) exponentials. (A) PS II cores of Thermosynechococcus elongatus, and from spinach: (B) BBY membrane, (C) LHCI-PSI, (D) stacked thylakoid membrane, (E) unstacked thylakoid membrane.

	0.3 ps	9 ps	21 ps	96 ps	0.50 ns	2.1 ns	3.9 ns	4.1 ns	inf	inf	Constraint	λ_{max} (nm)	identity
C_1 (yellow)	**0.968**										λ>674nm	659	Chl b
C_2 (dark green)	-0.698	**0.613**	0.052	0.016	0.012	0.007						683	Bulk Chl a
C_3 (black)	-0.200	-0.213	**0.395**	0.009	0.006	0.003						≈683/703	RC/P700
C_4 (green)	-0.006	-0.137	-0.034	**0.140**	0.024	0.012					λ>688nm	715	Red Chl a 1
C_5 (orange)	0.008	-0.230	-0.049	-0.097	**0.283**	0.084					λ>694nm	723	Red Chl a 2
C_6 (brown)	-0.075	-0.104	-0.021	-0.031	-0.190	**0.421**	0.001				λ>700nm	731	Red Chl a 3
C_7 (dark grey)		-0.005	-0.001	-0.001	-0.006	-0.027	**0.040**				λ>722nm	743	Red Chl a 4
C_8 (grey)								**0.032**			λ<722nm	675	Free LHC
C_9 (black dashed)	0.002	0.075	-0.339	-0.034	-0.113	-0.247	-0.001			**0.657**			RP
Ground State			-0.002	-0.001	-0.016	-0.253	-0.040	-0.032	**0.343**				

Table S1: The amplitude matrix of the model for the isolated LHCI-PSI complexes. A negative number indicates a rise of a component and a positive number indicates a decay. In bold the biggest contributors of decay for each compartment. Three rightmost columns contain zero constraint used ($SAS_{\#}(\lambda)=0$), λmax and identification of C# based upon the SAS.

C#	$k_{2\to\#}$	$k_{\#\to 2}$	ΔG (meV)
3	22	10	5.2
4	23	13	3.8
5	42	3.5	16
6	20	0.6	24
7	1	0.01	32

Table S2: Target analysis results of isolated LHCI-PSI complexes. Estimated rate constants and ΔG of the equilibria between bulk compartment C_2 and C_3-C_7 (T=77K, k_BT=6.6 meV)

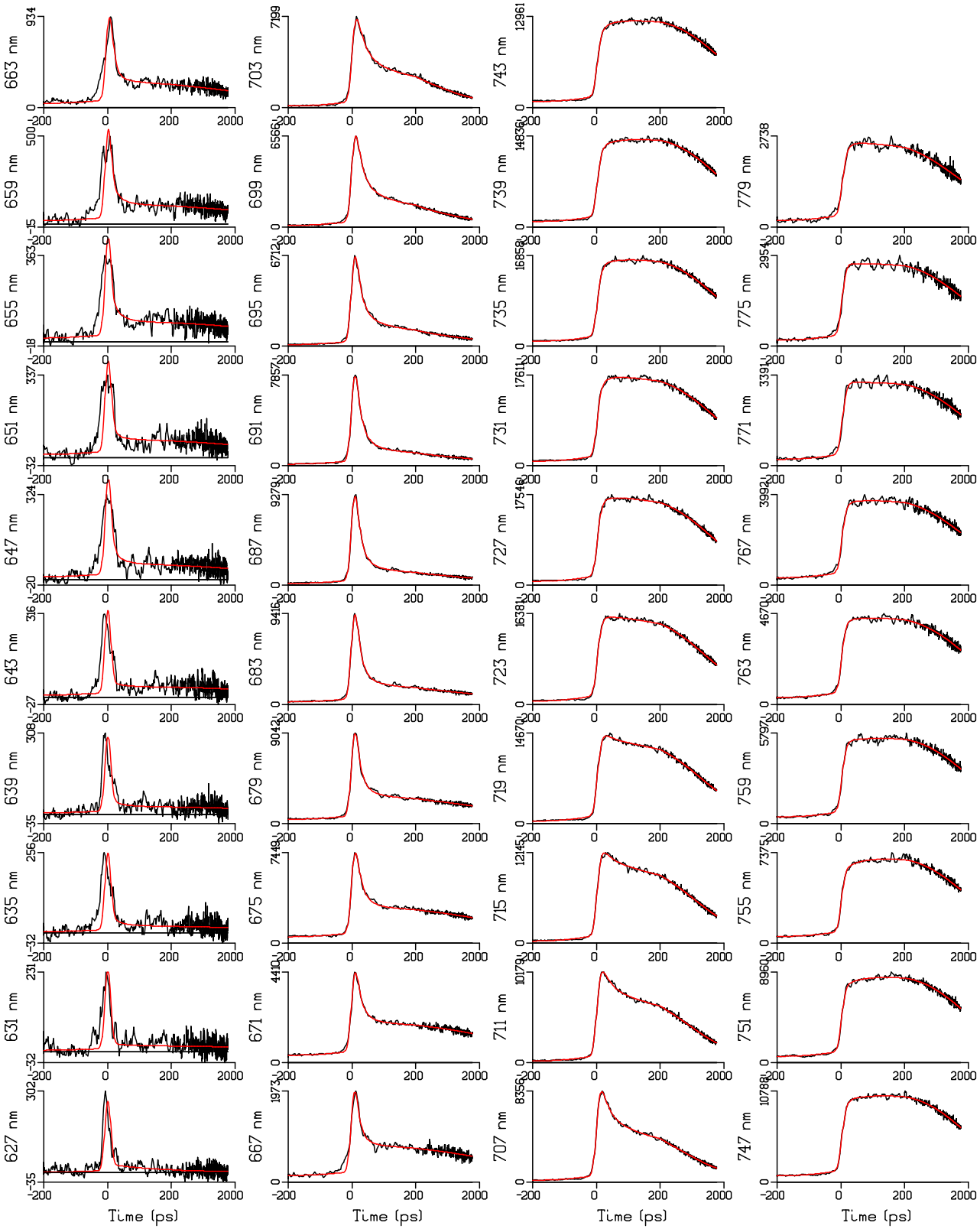

Figure S2: Time traces of fluorescence data of LHCI-PSI (black) and fit (red). Time axis is linear from -200 till 200 ps relative to the location of the IRF maximum, and logarithmic thereafter. Rms error of the fit was 82.

	4.4 ps	13.5 ps	29 ps	164 ps	0.58 ns	1.8 ns	4.0 ns	inf	inf	Constraint	λ_{max} (nm)	identity
C_1 (grey)	**0.171**	0.002	0.003	0.001							675	Ant1
C_2 (purple)	-0.214	0.243	**0.336**	0.120	0.012	0.040					684	Ant2
C_3 (blue)	0.044	-0.437	0.163	**0.258**	0.008	0.084					687	RC
C_4 (magenta)	0.004	-0.014	-0.043	-0.119	**0.196**	0.114					690	Red Chl
C_5 (cyan)		-0.002	-0.005	-0.010	-0.004	-0.065	0.112				696	Red Chl in CP47
C_6 (orange dashed)	-0.005	0.236	-0.617	**0.278**	-0.006	0.114	0.000			All λ	dark	RP1
C_7 (brown dashed)		-0.029	0.170	-0.587	-0.300	**0.742**	0.002			All λ	dark	RP2
C_8 (black dashed)			-0.004	0.068	0.122	-0.954	-0.007		**0.773**			RP3
Ground State		0.001	-0.003	-0.010	-0.029	-0.076	-0.109	**0.227**				

Table S3: The amplitude matrix of the model for the PSII core complexes. A negative number indicates a rise of a component and a positive number indicates a decay. In bold the biggest contributors of decay/rise for each compartment. The Ground State compartment has an infinite lifetime. Three rightmost columns contain zero constraint used ($SAS_{\#}(\lambda) = 0$), λ_{max}, and identification of C# based upon the SAS.

C#	$k_{2\to\#}$	$k_{\#\to 2}$	ΔG (meV)	C#	$k_{3\to\#}$	$k_{\#\to 3}$	ΔG (meV)	C#	$k_{6\to\#}$	$k_{\#\to 6}$	ΔG (meV)
3	39	18	5	6	25	18	2	7	9	1.2	13
4	4.1	1.8	6								
5	0.5	0.01	26								

Table S4: Target analysis results of PSII core complexes. Estimated rate constants and ΔG of the equilibria between the Ant2 compartment C_2 and C_3-C_5 (T=77K, k_BT=6.6 meV) and between RC (C_3) and RP1 (C_6) and RP1 and RP2 (C_7).

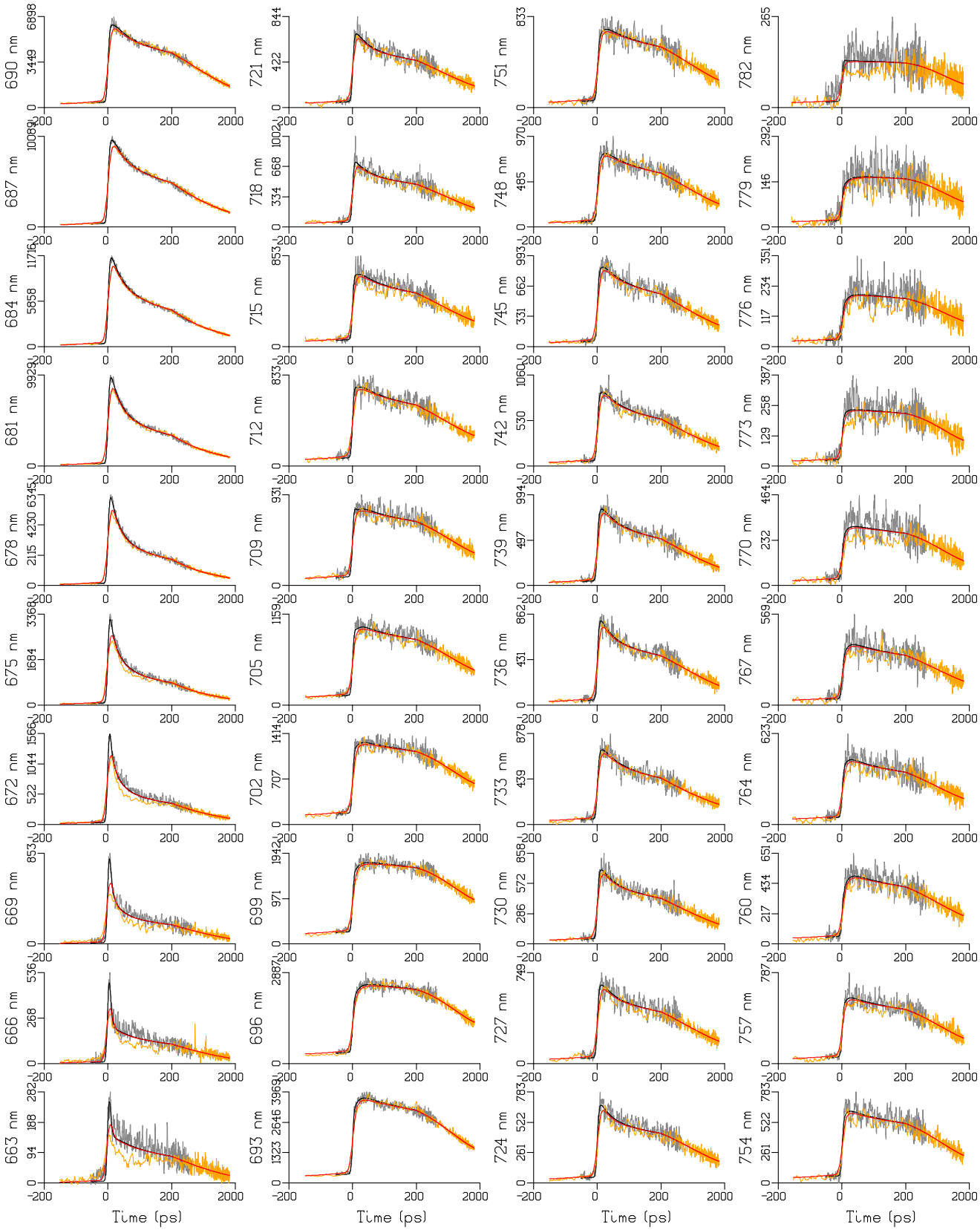

Figure S3: Time traces of fluorescence data of PSII core (grey and orange) and fit (black and red). Time axis is linear from -200 till 200 ps relative to the location of the IRF maximum, and logarithmic thereafter. Rms error of the fit was 63.

	7 ps	17.4 ps	37 ps	144 ps	0.52 ns	1.4 ns	4.0 ns	inf	inf	Constraint	λ_{max} (nm)	identity
C_1 (grey)	**0.322**										671	Ant1 (Chl b and blue Chl a)
C_2 (red)	-0.331	0.056	**0.337**	**0.479**	0.057	0.016					679	Ant2 (peripheral)
C_3 (blue)	0.011	-0.180	-0.264	**0.397**	0.070	0.022					683	Ant3 (core including RC)
C_4 (magenta)		0.014	0.045	-0.403	**0.309**	0.041					687	Red Chl CP43/CP47
C_5 (cyan)		0.002	0.005	-0.031	-0.022	-0.025	**0.073**				695	Red Chl in CP47
C_6 (orange dashed)	-0.002	0.163	-0.433	0.223	0.030	0.020				All λ	dark	RP1
C_7 (brown dashed)		-0.056	0.320	-0.726	-0.630	1.090	0.002			All λ	dark	RP2
C_8 (black dashed)		0.001	-0.009	0.077	0.237	-1.145	-0.005	0.844				RP3
Ground State			-0.001	-0.015	-0.051	-0.018	-0.070		0.156			

Table S5: The amplitude matrix of the model for the PSII membranes. A negative number indicates a rise of a component and a positive number indicates a decay. In bold the biggest contributors of decay for each compartment. Three rightmost columns contain zero constraint used ($SAS_{\#}(\lambda) = 0$), λ_{max}, and identification of C# based upon the SAS.

C#	$k_{2\to\#}$	$k_{\#\to 2}$	ΔG (meV)	C#	$k_{3\to\#}$	$k_{\#\to 3}$	ΔG (meV)	C#	$k_{6\to\#}$	$k_{\#\to 6}$	ΔG (meV)
3	17	12	2	6	18	18	0	7	19	0.3	27
				4	4.1	2.6	3				
				5	0.52	0.01	25				

Table S6: Target analysis results of PSII membrane complexes. Estimated rate constants and ΔG of the equilibria between antenna compartments C_3 (Ant 3) and C_2, C_4 and C_5 (T=77K, k_BT=6.6 meV) and between Ant 3 and RP1 (C_6) and between RP1 and RP2 (C_7).

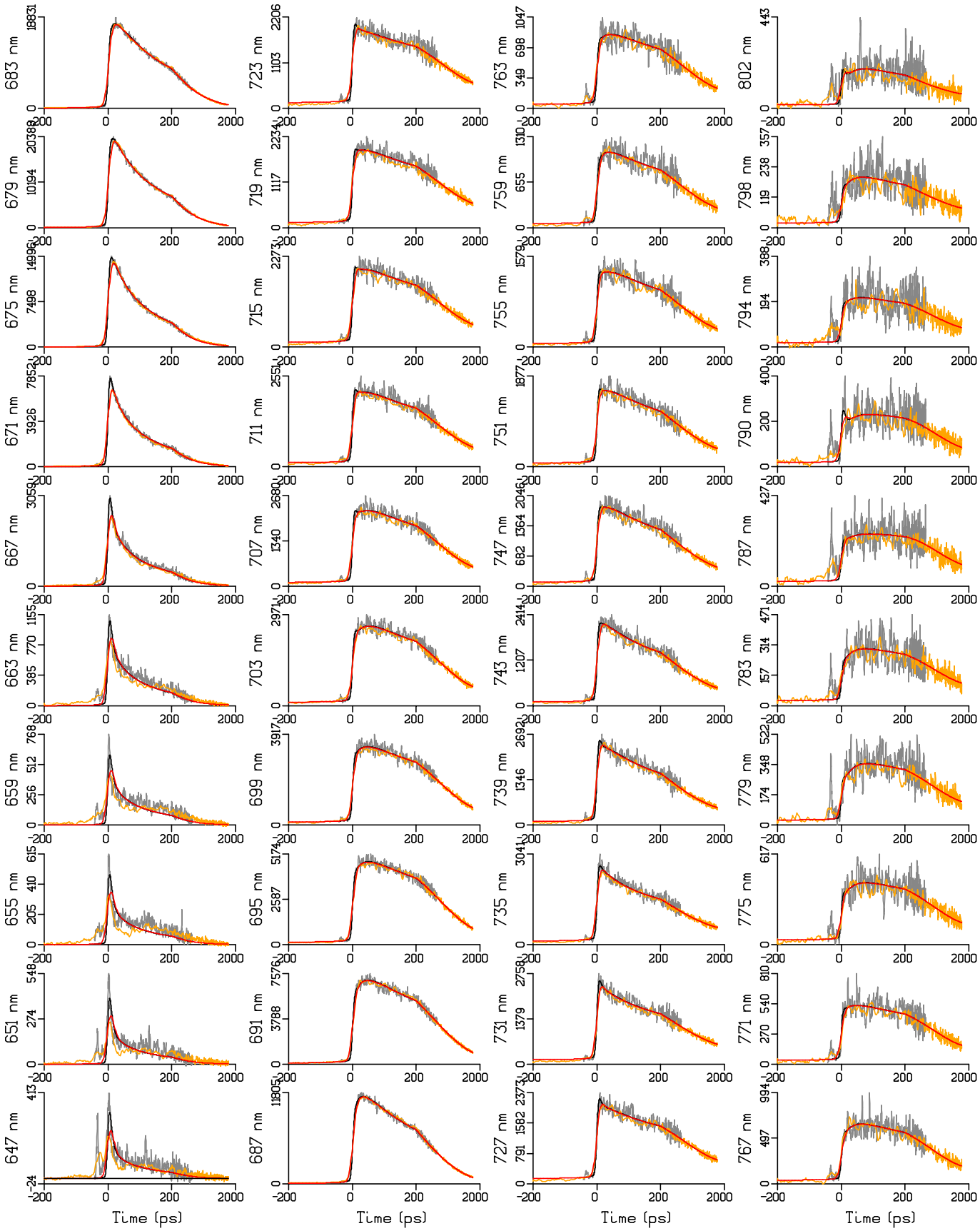

Figure S4:Time traces of fluorescence data of PSII membranes (grey and orange) and fit (black and red). Time axis is linear from -200 till 200 ps relative to the location of the IRF maximum, and logarithmic thereafter. Rms error of the fit was 102.

S	1 ps	18 ps	37 ps	114 ps	149 ps	429 ps	873 ps	2.7 ns	5.0 ns	inf	inf	inf	inf	Color	λ_{max} (nm)	identity
C_1	**1.000**													Yellow	683	Precursor
C_2	-0.399	**0.399**												Red	675	LHCII
C_3	-0.517	-0.011	**0.528**											Dark Green	679	PSI - 1
C_4	0.007	0.003	-0.350		**0.340**									Light Green	683	PSI - 2
C_5			0.088		-0.394		**0.306**							Orange	731	PSI – 3
C_6			-0.002		0.029		-0.181	**0.154**						Brown	735	PSI – 4
C_7	-0.099	-0.468		**0.567**										Blue	679	PSII – 1
C_8		0.034		-0.341		**0.306**								Magenta	683	PSII – 2
C_9				0.016		-0.058			**0.043**					Cyan	691	PSII – 3
RPI	0.007	0.003	-0.263		0.025		-0.104	-0.070		**0.402**					-	**RP PSI**
RPII		0.039		-0.237		-0.226					**0.424**				-	**RP PSII**
GSI			-0.002		0.001		-0.022	-0.084				**0.107**			-	
GSII		0.002		-0.006		-0.021			-0.043				**0.068**		-	

Table S7: The amplitude matrix of the model for the stacked and unstacked membranes, reported for the stacked membranes. A negative number indicates a rise of a component and a positive number indicates a decay. In bold the biggest contributors of decay for each compartment. The lifetimes of RPI (radical pair PSI), RPII (radical pair PSII), GS-I and GS-II (Ground states of PSI and PSII) are set to be infinite. Three rightmost columns contain the color coding used, λ_{max}, and identification of C# based upon the SAS.

U	1 ps	7.5 ps	37 ps	114 ps	149 ps	429 ps	873 ps	2.7 ns	5.0 ns	inf	inf	inf	inf	Color	λ_{max} (nm)	identity
C_1	**1.000**													Yellow	683	Precursor
C_2	-0.435	**0.435**												Red	675	LHCII
C_3	-0.463	-0.489	**0.952**											Dark Green	679	PSI - 1
C_4	0.006	0.051	-0.631		**0.574**									Light Green	683	PSI - 2
C_5		-0.002	0.159		-0.665		**0.509**							Orange	731	PSI – 3
C_6			-0.003		0.048		-0.300	**0.255**						Brown	735	PSI – 4
C_7	-0.115	-0.047		**0.162**										Blue	679	PSII – 1
C_8		0.001		-0.097		**0.096**								Magenta	683	PSII – 2
C_9				0.005		-0.018			**0.014**					Cyan	691	PSII – 3
RPI	0.006	0.048	-0.474		0.042		-0.172	-0.116		**0.665**					-	**RP PSI**
RPII	0.001	0.002		-0.068		-0.071					**0.136**				-	**RP PSII**
GSI		0.001	-0.004		0.001		-0.036	-0.139				**0.177**			-	
GSII				-0.002		-0.007			-0.014				**0.022**		-	

Table S8: The amplitude matrix of the model for the stacked and unstacked membranes, reported for the unstacked membranes. A negative number indicates a rise of a component and a positive number indicates a decay. In bold the biggest contributors of decay for each compartment. Three rightmost columns contain color coding used, λ_{max}, and identification of C# based upon the SAS.

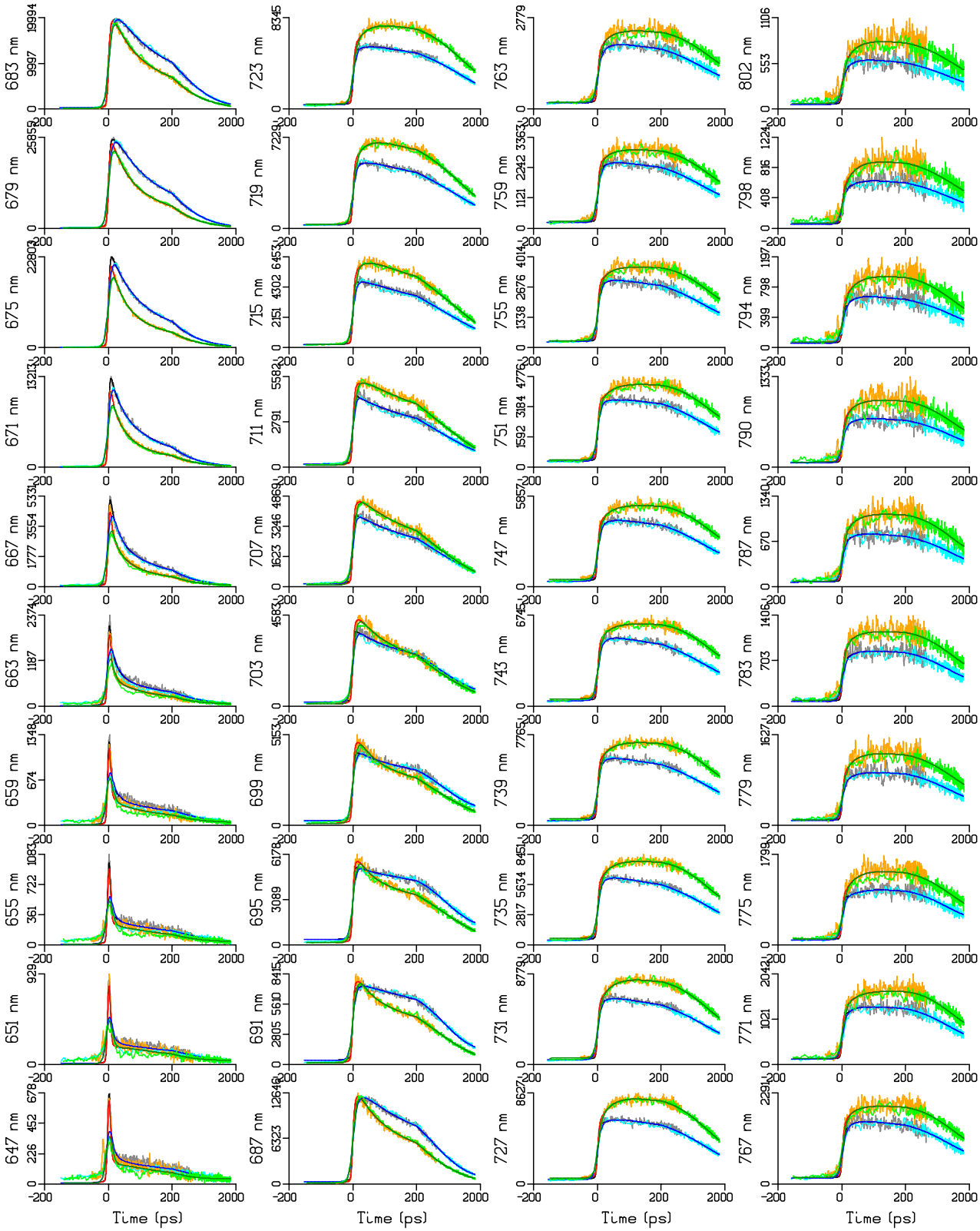

Figure S5: Time traces of fluorescence data of native (grey and cyan) and unstacked (light green and orange) thylakoid membranes and fit (black and blue for native, dark green and red for unstacked). Time axis is linear from -200 till 200 ps relative to the location of the IRF maximum, and logarithmic thereafter. Rms error of the fit was 112.

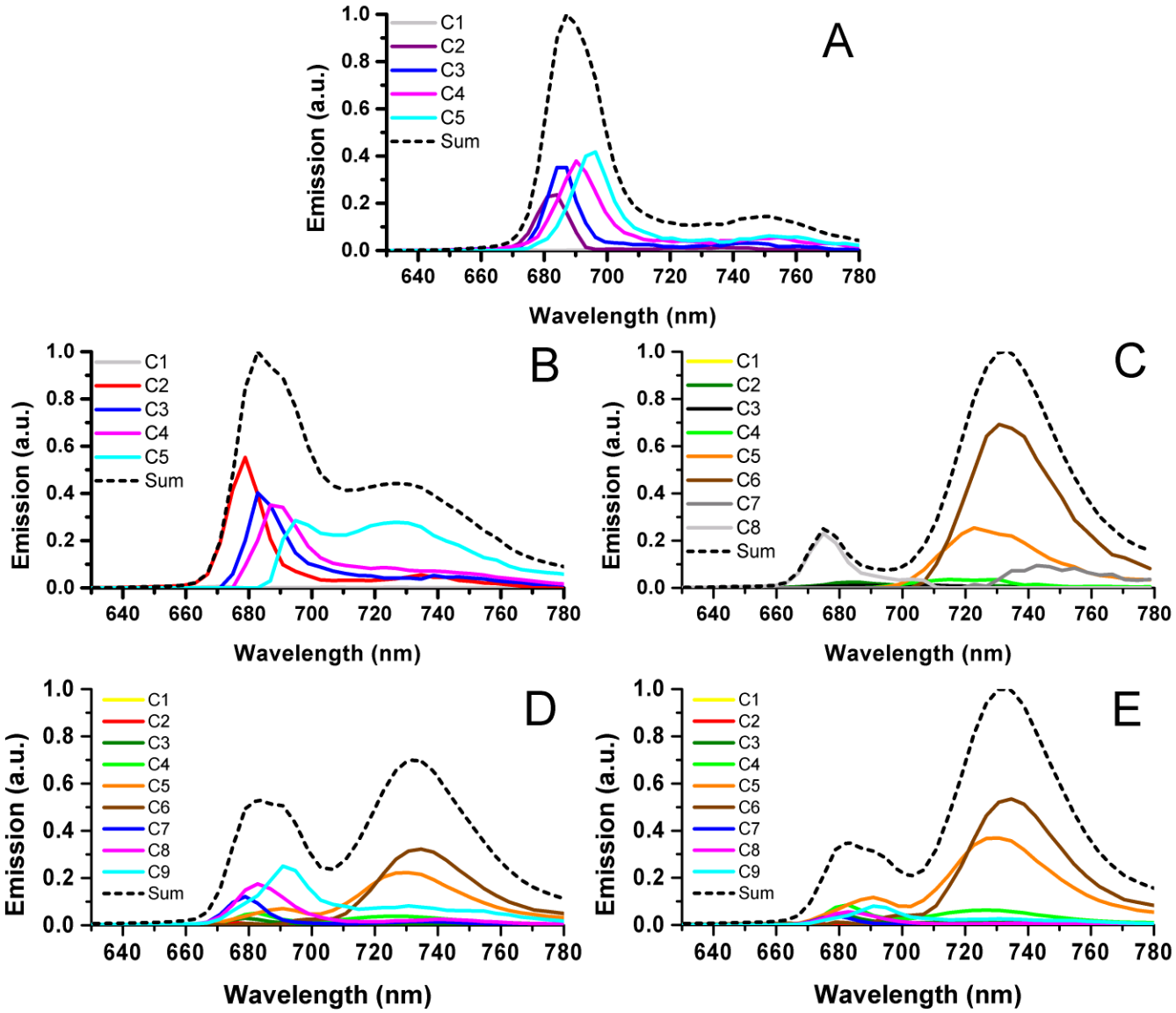

Figure S6. Reconstructed steady state emission at 77 K (black dashed) based on the target analysis. The contributions of each compartment are obtained by integrating the population profile over time, and multiplying this with the estimated SAS. The colors correspond with those in the target analysis figures. (A) PSII core, cf. Figure 3, of *Thermosynechococcus elongatus*, and from spinach (B) BBY membrane, cf. Figure 4, (C) LHCI-PSI, cf. Figure 2, (D) stacked thylakoid membrane, and (E) unstacked thylakoid membrane, both cf. Figure 5. Note that the same scale is used in D and E.